PHYSICS OF FLUIDS **26**, 112004 (2014)

Electrically generated eddies at an eightfold stagnation point within a nanopore

J. D. Sherwood,[1] M. Mao,[2] and S. Ghosal[2,3]
[1]*Department of Applied Mathematics and Theoretical Physics, University of Cambridge, Wilberforce Road, Cambridge CB3 0WA, United Kingdom*
[2]*Department of Mechanical Engineering, Northwestern University, 2145 Sheridan Road, Evanston, Illinois 60208, United States*
[3]*Department of Engineering Sciences and Applied Mathematics, Northwestern University, 2145 Sheridan Road, Evanston, Illinois 60208, United States*

(Received 15 July 2014; accepted 4 November 2014; published online 25 November 2014)

Electrically generated flows around a thin dielectric plate pierced by a cylindrical hole are computed numerically. The geometry represents that of a single nanopore in a membrane. When the membrane is uncharged, flow is due solely to induced charge electroosmosis, and eddies are generated by the high fields at the corners of the nanopore. These eddies meet at stagnation points. If the geometry is chosen correctly, the stagnation points merge to form a single stagnation point at which four streamlines cross at a point and eight eddies meet. © *2014 AIP Publishing LLC*. [http://dx.doi.org/10.1063/1.4901984]

I. INTRODUCTION

Streamline patterns reveal the topology of a flow field: we sketch streamlines, eddies, and stagnation points in order to develop our understanding of flows.[1,2] Stagnation points away from solid walls usually occur at the intersection of two streamlines, which divide the fluid into four separate regions. Such stagnation points can be generated in many ways, e.g., by a four-roll mill[3] or by opposed fluid jets in a cross-slot device.[4,5] More complicated stagnation points are harder to generate. Berry and Mackley[6] built a six-roll mill and investigated the flow field. When exact symmetry was achieved, six eddies met at a central point, and the various ways in which symmetry could be broken were described by Berry and Mackley[6] in terms of catastrophe theory. Here, we report an electrically generated flow field in which four streamlines cross at a point and divide the flow into eight regions.

The axisymmetric flow geometry is shown in Figure 1. A cylindrical hole of radius a passes through an uncharged thin dielectric plate of thickness h: the hole represents a nanopore in a membrane, and we are interested in the induced charge electroosmotic flow generated by an electric potential difference applied between the two sides of the membrane.[7–9] We set up cylindrical polar coordinates, with z axis along the axis of symmetry and with the plane surfaces of the membrane at $r > a$, $z = \pm h/2$.

In Sec. II, we consider the electric field passing through a circular hole in a membrane of zero thickness. We then (Sec. III) show how the field is modified at the edge of the hole when the membrane thickness h is small but non-zero. In Sec. IV, we review the fluid jets that are created by the electrical forces on the fluid near the corners of the membrane, and then in Sec. V we present numerical computations that show how the geometry of eddies created by these jets depends on the geometry of the hole in the membrane. As the ratio h/a increases, three stagnation points merge to form a stagnation point at which four streamlines cross. The stagnation points separate again as h/a increases further.

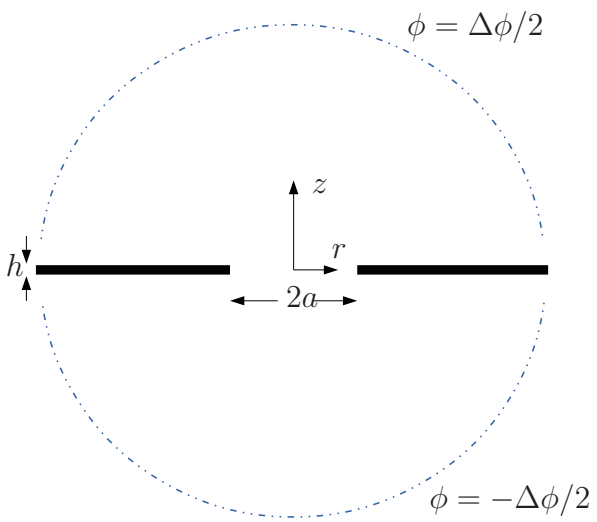

FIG. 1. The (infinite) dielectric plate of thickness h, pierced by a hole of radius a and surrounded by an electrolyte solution. The axisymmetric geometry represents a nanopore in a membrane. An electrical current is driven through the hole by a potential difference $\Delta\phi$ between the two sides, at infinity.

II. THE IMPOSED ELECTRIC FIELD

The pore and the two regions on either side of the membrane are occupied by an incompressible, electrically conducting Newtonian electrolyte solution with viscosity μ and electrical permittivity ϵ_f. The membrane is non-conducting, with permittivity ϵ_s. The electrical potential ϕ is continuous at the boundary between the solid membrane and the fluid. The surface charge density on the membrane is zero, so that $\epsilon \mathbf{n} \cdot \nabla\phi$ is continuous, where $\mathbf{n}$ is the unit normal to the membrane and the permittivity ϵ takes values ϵ_s and ϵ_f on the two sides of the boundary. If (as is usually the case) $\epsilon_s \ll \epsilon_f$, then to a first approximation we set $\epsilon_s = 0$, and $\mathbf{n} \cdot \nabla\phi = 0$ in the fluid adjacent to the membrane.

We assume that the electrolyte solution contains N ionic species, with valence z_i and number density n^i. Far from any charged surfaces, the ionic number densities are $n^i = n^i_\infty$, with $\sum_i z_i n^i_\infty = 0$ to ensure electrical neutrality of the bulk electrolyte. The electrical potential satisfies the Poisson equation

$$\nabla^2\phi = -\rho/\epsilon_f = -\sum_{i=1}^{N} e z_i n^i/\epsilon_f, \tag{1}$$

where ρ is the charge density.

Ions are convected with the fluid velocity $\mathbf{u}$, and move relative to the fluid under the influence of electric fields and thermal diffusion. The conservation equation for the number density n^i of the ith ionic species, in steady state, is therefore

$$\nabla \cdot \left[n^i \mathbf{u} - \omega_i (kT \nabla n^i + e z_i n^i \nabla\phi) \right] = 0, \tag{2}$$

where ω_i is the mobility of the ith species of ion, kT is the Boltzmann temperature, and e is the elementary charge. In the absence of any reactions at the surface of the membrane, the flux of ions normal to the membrane is zero at the membrane surface.

When $\epsilon_s = 0$, there is a steady solution of the ion conservation equation (2) in which the fluid is at rest ($\mathbf{u} = 0$), the ionic number densities are unperturbed ($n^i = n^i_\infty$), and the electrical potential $\phi = \phi_0$ within the electrolyte is given by the solution of the Laplace equation

$$\nabla^2\phi_0 = 0, \tag{3a}$$

$$\mathbf{n} \cdot \nabla\phi_0 = 0 \qquad \text{on the membrane surface,} \tag{3b}$$

$$\phi \to \pm\Delta\phi/2, \quad \text{as } \mathbf{r} \to \infty \text{ in } z \gtrless 0. \tag{3c}$$

This represents Ohmic conduction through an electrolyte with uniform electrical conductivity. The solution $\phi_0 = \Phi_0$ of the Laplace equation (3) when $h = 0$ is given by Morse and Feshbach[10] (p. 1292) in terms of oblate spherical coordinates (ξ, η) where $-\infty < \xi < \infty$, $0 \le \eta \le \pi/2$ such that

$$z = a \sinh\xi \cos\eta \quad , \quad r = a \cosh\xi \sin\eta, \tag{4}$$

and is

$$\phi_0 = \Phi_0(r, z) = \frac{\Delta\phi}{2}\left[1 - \frac{2}{\pi}\tan^{-1}\left(\frac{1}{\sinh\xi}\right)\right], \quad z > 0, \quad h = 0, \tag{5a}$$

$$= -\Phi_0(r, -z), \quad z < 0. \tag{5b}$$

On the surface $z = 0_+$ of the membrane

$$\Phi_0(r, 0_+) = \frac{\Delta\phi}{2}\left[1 - \frac{2}{\pi}\tan^{-1}\left(\frac{a}{(r^2 - a^2)^{1/2}}\right)\right], \quad r > a, \tag{6}$$

and for $r = a(1 + \delta)$, with $\delta \ll 1$,

$$\Phi_0(r, 0_+) \approx \frac{\Delta\phi}{\pi}(2\delta)^{1/2}, \tag{7}$$

with $\Phi_0(r, 0_-) = -\Phi_0(r, 0_+)$. The electric field in the plane of the hole is

$$\mathbf{E} = -\frac{\Delta\phi\ \hat{\mathbf{z}}}{\pi a\left(1 - r^2/a^2\right)^{1/2}}, \quad r < a, \tag{8}$$

and if the conductivity of the electrolyte is Σ, the total current through the hole is $2a\Sigma\Delta\phi$. However, real membranes have a non-zero thickness $h > 0$. We shall show in Sec. III that when $0 < h \ll a$, the potential ϕ_0 differs from the potential Φ_0 for $h = 0$ by an amount $O((h/a)^{1/2})$. We neglect this perturbation for the moment, and assume $\phi_0(r, h/2) \approx \Phi_0(r, 0_+)$. The leading order potential ϕ_0 leads to an electric field of strength

$$\hat{\mathbf{z}} \cdot \nabla\phi = \frac{2\phi_0(r, h/2)}{h} \approx \frac{2\Phi_0(r, 0_+)}{h} \tag{9}$$

within the membrane.

If $\epsilon_s = 0$ (as assumed so far), the electric field (9) within the membrane and the electric field (3b) outside the membrane satisfy the requirement that $\epsilon\mathbf{n} \cdot \nabla\phi$ should be continuous at the boundary. However, in the real world, ϵ_s is at least as large as the permittivity of free space, ϵ_0, so that $\epsilon_s \ge \epsilon_0 > 0$, and the normal electric field outside the membrane must be perturbed at $O(\epsilon_s\Delta\phi/(\epsilon_f h))$ in order to ensure continuity of $\epsilon\mathbf{n} \cdot \nabla\phi$. Ions move toward (or away from) the membrane under the influence of this perturbation until equilibrium, with zero flux of ions into the membrane, is achieved. In order to determine this perturbation to the field, we assume that

$$\gamma = \frac{\epsilon_s}{\epsilon_f} \ll 1 \tag{10}$$

and use γ as the basis for a perturbation expansion

$$\phi = \phi_0 + \gamma\phi_1 + \cdots, \tag{11a}$$

$$n^i = n_0^i + \gamma n_1^i + \cdots, \tag{11b}$$

$$\mathbf{u} = \quad \gamma\mathbf{u}_1 + \cdots, \tag{11c}$$

where the subscript 0 refers to the uniform ion density $n_0^i = n_\infty^i$ and to the potential (3c) for $\epsilon_s = 0$. The $O(\gamma)$ terms in the steady-state ion conservation equation give

$$\mathbf{u}_1 \cdot \nabla n_0^i = \omega_i \nabla \cdot \left[ez_i n_0^i \nabla\phi_1 + ez_i n_1^i \nabla\phi_0 + kT\nabla n_1^i\right]. \tag{12}$$

Since n_0^i is uniform, the left-hand side of (12) is zero.

On the surface of the membrane (except close to the edge of the hole), the potential ϕ_0 varies on a length scale $r > a$, whereas we expect the perturbation potential ϕ_1 to vary on the Debye length scale

$$\kappa^{-1} = \left(\frac{\epsilon_f kT}{\sum_{i=1}^{N} e^2 z_i^2 n_\infty^i} \right)^{1/2}. \tag{13}$$

Hence, if $r - a \gg \kappa^{-1}$ so that we are much further than a Debye length away from the edge of the hole, we may neglect the second term on the right-hand side of (12), which reduces to

$$\nabla \cdot \left[e z_i n_0^i \nabla \phi_1 + kT \nabla n_1^i \right] = 0. \tag{14}$$

The perturbed ionic number densities are therefore given by a Boltzmann distribution

$$n_1^i = n_\infty^i \mathrm{e}^{-e z_i \phi_1 / kT} \tag{15}$$

and ϕ_1 satisfies the Poisson equation

$$\nabla^2 \phi_1 = -\frac{\rho_1}{\epsilon_f} = -\frac{e}{\epsilon_f} \sum_{i=1}^{N} z_i n_1^i = -\frac{e}{\epsilon_f} \sum_{i=1}^{N} z_i n_\infty^i \mathrm{e}^{-e z_i \phi_1 / kT}. \tag{16}$$

The perturbation potential ϕ_1 varies in the z direction over the Debye length scale κ^{-1}, and we neglect its slow variation with r. We assume that $\gamma e \phi_1/(kT)$ is small, and linearize the Poisson-Boltzmann equation (16), which becomes

$$\frac{\mathrm{d}^2 \phi_1}{\mathrm{d}z^2} = -\kappa^2 \phi_1. \tag{17}$$

The solution of (17) that ensures that the potential $\phi = \phi_0 + \gamma \phi_1$ satisfies the jump boundary condition $[\epsilon \mathbf{n} \cdot \nabla \phi] = 0$ at the surface of the membrane is

$$\phi = \phi_0 - \frac{2\Phi_0(r, 0_+)\epsilon_s}{h\kappa\epsilon_f + 2\epsilon_s} \exp[-\kappa(z - h/2)], \qquad z > h/2, \tag{18a}$$

$$\phi = \phi_0 + \frac{2\Phi_0(r, 0_+)\epsilon_s}{h\kappa\epsilon_f + 2\epsilon_s} \exp[\kappa(z + h/2)], \qquad z < -h/2, \tag{18b}$$

with

$$\phi = \frac{2\Phi_0(r, 0_+)\kappa\epsilon_f z}{h\kappa\epsilon_f + 2\epsilon_s}, \qquad |z| < h/2, \tag{19}$$

inside the solid membrane. We see from (18) that the perturbation $\gamma\phi_1$ is only small compared to ϕ_0 if $\gamma/(h\kappa) \ll 1$. We also note that (18) does not represent the first terms of a systematic expansion, and is incorrect at $O((\gamma/h\kappa)^2)$. However, we prefer to leave the expansion in the form (18) since it shows explicitly how the expansion fails in the limit $h \to 0$. In particular, far from the hole we recover the uniform charge cloud that would be induced in the absence of any hole. A detailed analysis of induced charge electroosmotic flow around an uncharged dielectric sphere (or cylinder) of radius a in the limit $a\kappa \gg 1$ has been provided by Schnitzer and Yariv.[11]

The perturbation potential (18) outside the membrane can be described in terms of an effective induced zeta potential

$$\zeta_i = -\frac{2\epsilon_s \Phi_0(r, 0_+)}{h\kappa\epsilon_f + 2\epsilon_s}. \tag{20}$$

The tangential electric field $-\partial\phi/\partial r$ acts on the charge cloud adjacent to the membrane and causes a tangential velocity. Immediately outside the double layer (assuming $r \gg a + \kappa^{-1}$, so that flow can be assumed to be locally one-dimensional), the leading-order radial fluid velocity outside the charge cloud is given by the Smoluchowski slip velocity

$$u = \frac{\partial\phi}{\partial r}\frac{\epsilon_f \zeta_i}{\mu}, \tag{21}$$

and using the expansion (7) at $r = a(1+\delta)$, together with (20), we obtain, in the limit $\epsilon_s \ll h\kappa\epsilon_f$,

$$u = -\frac{2\epsilon_s}{ah\kappa\mu}\left(\frac{\Delta\phi}{\pi}\right)^2, \qquad z = 0_+. \tag{22}$$

The radial velocity created by the induced charge is toward the hole on both sides of the membrane.

This solution (18), (19), (22) is clearly inappropriate within a distance $O(\kappa^{-1})$ of the edge of the hole, where the electric field can no longer be assumed to vary slowly with r. In Sec. III, we find a local solution to the Laplace equation in the neighbourhood of the edge, for the case $\epsilon_s = 0$ for which the electric field satisfies a Neumann boundary condition (3b) at the surface of the membrane.

III. MEMBRANE OF UNIFORM THICKNESS: A CONFORMAL MAPPING SOLUTION

We now study in detail the electric field at the edge of the membrane of thickness $h > 0$ near $r = a$, for the case $\epsilon_s = 0$. Sufficiently close to the edge (Figure 2(b)) we neglect the azimuthal curvature, and seek a local solution of the two-dimensional Laplace equation. In the limit $h \ll a$, the outer limit of the local solution can then be matched to the inner limit (7) of the outer solution for a membrane of zero thickness.

We map the upper half of the Z-plane $Z = X + \mathrm{i}Y$ (Figure 2(a)) onto the region outside a rectangular edge in the w plane $w = u + \mathrm{i}v$ (Figure 2(b)) by means of the conformal mapping[12]

$$w = H\left[Z(Z^2-1)^{1/2} - \cosh^{-1}(Z)\right], \tag{23}$$

where the constant H will be determined later, and the branch of the square root is chosen such that

$$w = H\left[X(X^2-1)^{1/2} - \ln(X + (X^2-1)^{1/2})\right], \quad Z = X \geq 1, \tag{24}$$

along the real axis. The rectangular edge (Figure 2(b)) represents the right-hand edge of the hole in the membrane (Figure 1), seen on a scale at which the membrane thickness can be observed, and the constant H in (23) will eventually be chosen to ensure that the membrane has thickness h.

If $Z = X \gg 1$ (E on Figure 2(a)),

$$w \sim HX^2. \tag{25}$$

If $Z = 1 + \varepsilon$, with $|\varepsilon| \ll 1$ (near D on Figure 2(a)), then

$$w = H\left(\frac{4\sqrt{2}}{3}\right)\varepsilon^{3/2}, \tag{26}$$

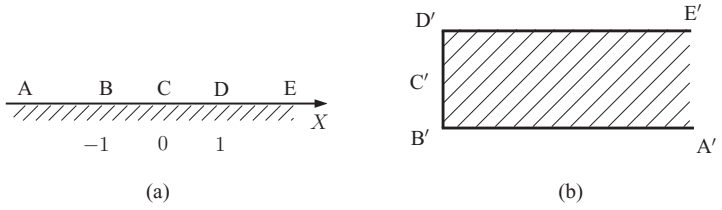

(a) (b)

FIG. 2. (a) The Z plane, with origin at C. D is at $Z = 1$ and B at $Z = -1$. (b) The w plane, with origin at D′. C′ is at $w = -\mathrm{i}H\pi/2$ and B′ is at $w = -\mathrm{i}H\pi$. The w plane represents the edge of the hole in the membrane.

so that if $Z = 1 - \varepsilon_R$, with $0 < \varepsilon_R \ll 1$ real,

$$w = -H\left(\frac{4\sqrt{2}}{3}\right)\varepsilon_R^{3/2}\mathrm{i}, \tag{27}$$

and if $Z = \varepsilon$ with $|\varepsilon| \ll 1$ (near C on Figure 2(a)),

$$w = -\mathrm{i}H\left[\frac{\pi}{2} - 2\varepsilon\right]. \tag{28}$$

Finally, since $\cosh^{-1}(-Z) = \pi\mathrm{i} - \cosh^{-1}Z$, we note that when $Z = -1$ (at B),

$$w = -H\cosh^{-1}Z = -\mathrm{i}H\pi. \tag{29}$$

In order to map the upper half Z plane into the space outside a semi-infinite rectangular slab of thickness $|\mathrm{D'B'}| = h$, we see from (26) and (29) that we should choose $H = h/\pi$.

We now consider the (harmonic) function

$$\phi = CH^{1/2}\Re(Z) = CH^{1/2}X. \tag{30}$$

This satisfies the Neumann boundary condition (3b) on the boundary ABCDE in the Z plane, and after transformation to the w plane leads to a solution[10] of the Laplace equation that satisfies the Neumann boundary condition on the transformed boundary A′B′C′D′E′, i.e., on the boundary of the membrane near the edge of the hole. In the far field of the w plane,

$$\phi = C\Re(w^{1/2}), \tag{31}$$

which matches with the inner expansion of the outer solution (7) for the electric potential at the edge of the hole in a membrane of zero thickness if

$$C = \left(\frac{2}{a}\right)^{1/2}\frac{\Delta\phi}{\pi}. \tag{32}$$

Close to the corner D′ of the slab, at $w = s\,\mathrm{e}^{\mathrm{i}\theta}$ with $s \ll 1$,

$$\phi = CH^{1/2}\left\{1 + \left(\frac{3s}{4H\sqrt{2}}\right)^{2/3}\cos\left(\frac{2\theta}{3}\right)\right\}. \tag{33}$$

Thus, the electrical potential at the corner D′ is $CH^{1/2} = \Delta\phi(2h/a)^{1/2}\pi^{-3/2}$, together with an eigen-solution proportional to s^λ, with $\lambda = 2/3$, and the potential difference between the two corners D′ and B′ (Figure 2) is

$$\Delta\phi_c = \Delta\phi\left(\frac{2}{\pi}\right)^{3/2}\left(\frac{h}{a}\right)^{1/2}. \tag{34}$$

In Sec. IV, we compare the magnitude of the electroosmotic flow generated at the corner by the potential (33) with the magnitude of the flow (22) generated along the surface of the membrane away from corners at the edge of the hole.

IV. INDUCED CHARGE AT A CORNER

The theory of electro-osmotic flow at a dielectric corner is discussed by Thamida and Chang[13] and Yossifon *et al.*[14] We consider a plane 2-dimensional wedge of internal angle $2\alpha = 2(\pi - \theta_0)$, and adopt plane polar coordinates (s, θ), as shown in Figure 3. The solution of the Laplace equation for the potential ϕ outside the electrical double layer, antisymmetric in θ outside the wedge, has the form

$$\phi = As^\lambda \sin\lambda\theta. \tag{35}$$

Zero flux of ions into the solid wedge requires

$$\mathbf{n}.\nabla\phi = \frac{1}{s}\frac{\partial\phi}{\partial\theta} = A\lambda s^{\lambda-1}\cos\lambda\theta = 0, \quad \theta = \theta_0 = \pi - \alpha, \tag{36}$$

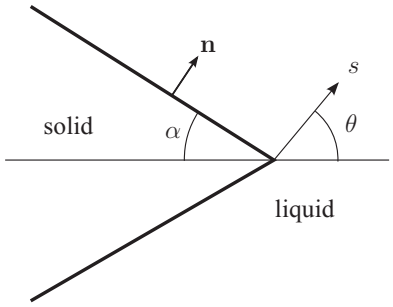

FIG. 3. A dielectric wedge, of angle 2α, with local cylindrical coordinates (s, θ).

so that

$$\lambda = \frac{(2n+1)\pi}{2\theta_0}, \qquad n = 0, \pm 1, \pm 2 \ldots . \tag{37}$$

If $\theta_0 = \pi$, the least singular eigensolution (35) corresponds to $\lambda = 1/2$, in agreement with (7). If $\alpha = \pi/4$, so that $\theta_0 = 3\pi/4$, then $\lambda = 2/3$, as found in (33), and

$$A = \frac{3^{2/3}}{2^{5/3}} C H^{-1/6} = \frac{3^{2/3}}{2^{7/6}} \frac{\Delta\phi}{\pi a^{1/2}} \left(\frac{\pi}{h}\right)^{1/6}. \tag{38}$$

Within the solid wedge, the potential is

$$\phi = \phi_w = A s^{\lambda} \frac{\sin \lambda\theta_0}{\sin \lambda\alpha} \sin[\lambda(\pi - \theta)], \tag{39}$$

which is antisymmetric about $\theta = \pi$. As in Sec. II, we conclude that there will be an induced surface charge, corresponding to an induced zeta potential

$$\zeta_i = -\frac{\epsilon_s}{\kappa \epsilon_f} \frac{\partial \phi_w}{\partial n} = -\frac{\epsilon_s}{\epsilon_f} \frac{A s^{\lambda-1}}{\kappa} \lambda \cot \lambda\alpha \ \sin \lambda\theta_0, \quad \theta = \theta_0, \tag{40a}$$

$$= \frac{\epsilon_s}{\epsilon_f} \frac{A s^{\lambda-1}}{\kappa} \lambda \cot \lambda\alpha \ \sin \lambda\theta_0, \quad \theta = -\theta_0. \tag{40b}$$

Note that this potential becomes large as $s \to 0$ close to the apex of the wedge, and an analysis based on linearized Poisson-Boltzmann theory therefore breaks down. Large induced potentials on the surface of a spherical particle are discussed by Yariv and Davis.[15]

The tangential electric field immediately outside the wall is

$$E_s = -\frac{\partial \Phi_l}{\partial s} = \lambda A s^{\lambda-1} \sin \lambda\theta_0, \quad \theta = \theta_0, \tag{41a}$$

$$= -\lambda A s^{\lambda-1} \sin \lambda\theta_0, \quad \theta = -\theta_0, \tag{41b}$$

and, as discussed in Sec. II, this acts upon the charge cloud associated with the induced zeta potential ζ_i (40). If the Debye length κ^{-1} is sufficiently small, we expect a Smoluchowski slip velocity just outside the charge cloud, of magnitude

$$u_s = -\frac{\epsilon_f E_s \zeta_i}{\mu} = -\frac{\epsilon_s}{\kappa\mu} A^2 s^{2\lambda-2} \lambda^2 \cot \lambda\alpha \ \sin^2 \lambda\theta_0, \quad \theta = \pm\theta_0. \tag{42}$$

For the corner of the membrane at the entrance to the pore, $\alpha = \pi/4$ and $\lambda = 2/3$, with A given by (38), so that the velocity is

$$u_s = -\frac{\epsilon_s}{a\kappa\mu} s^{-2/3} \left(\frac{\Delta\phi}{\pi}\right)^2 \left(\frac{\pi}{h}\right)^{1/3} 3^{-1/6} 2^{-1/3}, \quad \theta = \pm\theta_0. \tag{43}$$

We can seek a solution of the Stokes equations for fluid flow around the corner which has the required radial velocity $u_s \propto s^{2\lambda-2}$, and look for a stream function ψ of the form[2] (for $m \neq 0, 1, 2$)

$$\psi = s^m \left[B_1 e^{im\theta} + B_2 e^{i(m-2)\theta} \right], \tag{44}$$

where the B_i are constants. The fluid velocity is then

$$u_s = \frac{1}{s}\frac{\partial \psi}{\partial \theta} \quad , \quad u_\theta = -\frac{\partial \psi}{\partial s}. \tag{45}$$

However, we shall not proceed further with this local solution, since in Sec. V we consider full numerical solutions of the governing equations.

Note that a direct comparison between u_s (43) and the slip velocity u (22) away from the the edge of the hole indicates that $u > u_s$ for $s > 0.337h$, so that any solution of the form (44) is only useful very close to the corner.

V. NUMERICAL COMPUTATION OF EDDIES

The set of time-independent equations governing the electrical potential ϕ, the ionic number densities n^i, the fluid velocity $\mathbf{u}$, and fluid pressure p consists of the Poisson equation (1), the ion conservation equation (2), and the Stokes equations

$$-\nabla p + \mu \nabla^2 \mathbf{u} - \nabla\phi \sum_{i=1}^{N} z_i e n^i = 0, \tag{46}$$

$$\nabla \cdot \mathbf{u} = 0. \tag{47}$$

We solve the coupled equations (1), (2), (46), and (47) by means of a finite volume numerical scheme based upon the OpenFOAM CFD library.[16] The surface charge density $\sigma_{\rm m}$ in the absence of any imposed field is set to zero, and a symmetrical electrolyte ($N = 2$, $z_1 = -z_2 = 1$) is considered, with identical cationic and anionic mobilities. There is therefore complete symmetry about the plane of the membrane, and no net flow through the hole. The relative permittivity of the electrolyte is $\epsilon_f/\epsilon_0 = 80$, where ϵ_0 is the permittivity of free space, and that of the membrane is set in the computations to be either $\epsilon_s/\epsilon_0 = 3.9$, corresponding to silica, or $\epsilon_s = 0$. The hole has radius $a = 5$ nm (a typical hole size in silica[17] or graphene[18,19]), with $a\kappa = 5$, corresponding to an electrolyte of strength 95 mM (at 300 K). The results presented here were performed with a mesh spacing that varied smoothly from $\kappa^{-1}/10$ close to the membrane and hole, to κ^{-1} at the far outer boundary. The potential difference applied to generate the flow was $\Delta\phi = 1$ mV, so that $e\Delta\phi/kT \approx 0.04$: fluid velocities are everywhere proportional to $(\Delta\phi)^2$ as long as $e\Delta\phi/kT$ is sufficiently small for the linearized Poisson-Boltzmann equation to be valid, in which case the streamlines are independent of $\Delta\phi$. Further details of the computational scheme are given by Mao *et al.*[8]

The difference in electrical potential between the two ends of the pore, at the wall of the cylindrical pore, is $\Delta\phi_c$ (34) when $h \ll a$ and this analytic prediction is shown in Figure 4 as a function of h/a. We see that the analytic result is in good agreement with computed results $\Delta\phi_{c,0}$ ($\epsilon_s = 0$) for $h/a < 0.4$. Also shown are computations for a membrane with relative permittivity $\epsilon_s/\epsilon_0 = 3.9$, which differ little from those for $\epsilon_s/\epsilon_0 = 0$. If h/a is sufficiently small, the resistance of the pore changes only slightly[9] from that predicted for the electric field (5b) when $h = 0$. We therefore expect the current along the centreline of the pore, well away from the edges, to be little changed, and the electric field along the centreline is still (to a first approximation) $-\hat{\mathbf{z}}\Delta\phi/(a\pi)$ (8). The potential difference between the ends ($z = \pm h/2$) of the pore along the centreline should therefore be

$$\Delta\phi_x = \frac{\Delta\phi}{\pi}\left(\frac{h}{a}\right), \quad h \ll a. \tag{48}$$

This too is shown in Figure 4, and we see reasonable agreement between theory and computation.

When $\epsilon_s/\epsilon_0 = 3.9$, induced charges lead to electro-osmosis. Streamlines computed for the case $h = 0.4a$ are shown in Figure 5(a) and take the form shown schematically in Figure 6(a). Axial symmetry implies that ABD and GFH in Figure 6(a) are cross-sections of the same toroidal eddy

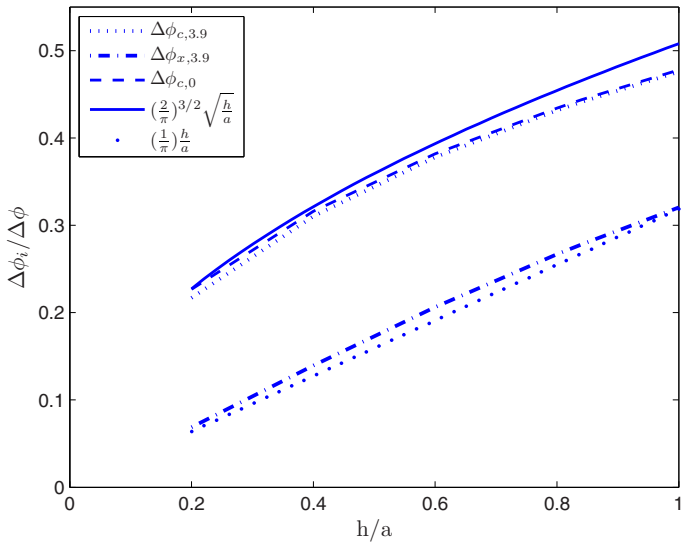

FIG. 4. The potential difference across the cylindrical pore, scaled by the total potential difference $\Delta\phi$ between the two sides of the membrane. Potential difference along the pore wall: ——— theoretical prediction $\Delta\phi_c$ (34); – – – – $\Delta\phi_{c,0}$ computed for $\epsilon_s = 0$; $\cdots$ computed for $\epsilon_s/\epsilon_0 = 3.9$. Potential difference along the pore axis: - - - - - - - $\Delta\phi_{c,3.9}$ theoretical prediction $\Delta\phi_x$ (48); – – – – – computed $\Delta\phi_{x,3.9}$ for $\epsilon_s/\epsilon_0 = 3.9$.

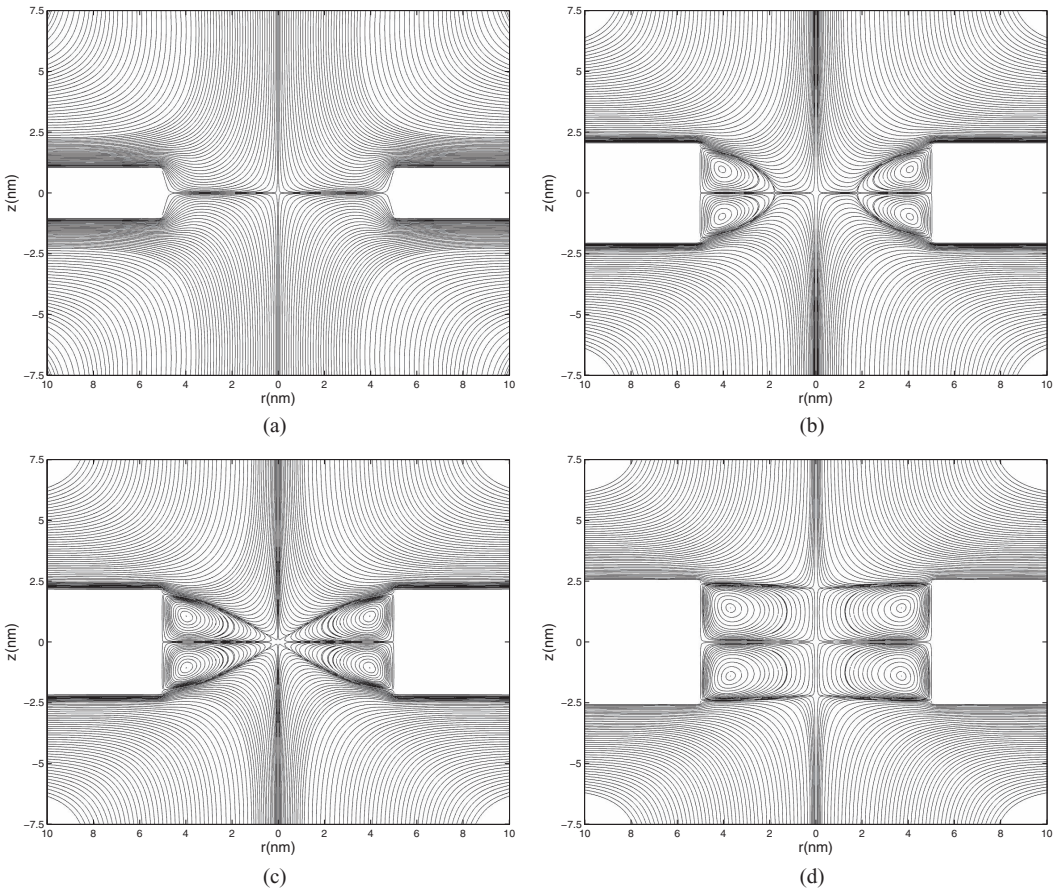

FIG. 5. Numerically computed streamlines in the neighbourhood of the hole, $a\kappa = 5$, $\epsilon_s/\epsilon_0 = 3.9$. Uncharged membrane of thickness: (a) $h = 0.4a$; (b) $h = 0.8a$; (c) $h = 0.84a$; (d) $h = a$.

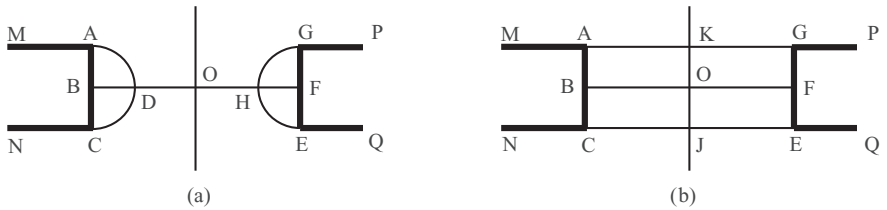

FIG. 6. Schematic showing the boundaries of eddies in Figure 5. MA and GP represent the membrane surface at $z = h/2$; NC and EQ the surface at $z = -h/2$. ABC and GFE represent the cylindrical surface of the nanopore. Stagnation points within fluid (away from the walls) are at (a) O,D,H and (b) O,J,K. Axial symmetry implies that the eddies ABD and GFH in (a) are cross-sections of the same toroidal eddy.

(and similarly for CBD and EFH). However, the eddy pairs ABCD and EFGH in Figure 5(a) are very small. Flow near the corners A,C,E,G is a combination of the horizontal velocity (22) predicted on the upper and lower surfaces of the membrane, and the local corner flow (43), which flows upwards along BA and FG, thereby causing the horizontal flow to separate at A and G (and similarly at C and E). At fixed position, the uniform flow (22) varies as h^{-1}, whereas the corner flow (43) varies as $h^{-1/2}$. As h increases, the ratio of the corner flow to horizontal flow increases, and the eddies become larger, so that the stagnation points D and H (or more correctly, stagnation lines, since the flow has axial symmetry) move toward the central stagnation point at O. This is seen in Figure 5(b) for $h = 0.8a$.

When $h \approx 0.84a$ the stagnation points D and H merge into O, and 8 eddies meet at O, as seen in Figure 5(c). Any further increase in h causes the stagnation point to bifurcate into three points, at O, J, and K, as seen in Figure 5(d) and shown schematically in Figure 6(b). Figure 5(c) shows eddies for $h = 0.84a$, and the precise value for h at which the 8-fold stagnation point is formed lies within the range $0.83a < h < 0.85a$. Computations with larger grid size $\kappa^{-1}/5$ in the vicinity of the membrane gave streamlines that could not be distinguished from those in Figure 5, and the 8-fold stagnation point was still formed at $h \approx 0.84a$,

The Debye length when $h = 0.84a$ and $a\kappa = 5$ is $\kappa^{-1} = 0.238h$. The corner flow discussed in Sec. IV is valid only outside the charge cloud (i.e., for $s > \kappa^{-1}$), in which region the corner flow (45) is swamped by the velocity (22) parallel to the plane of the membrane. We are therefore unable to see in Figure 5 regions close to the corners in which streamlines are symmetric about the local coordinate $\theta = 0$ (Figure 3).

Any asymmetry in the flow caused by a non-zero surface charge density σ_m or by differences between the mobilities of the ions causes a net flow from one side of the membrane to the other. If this is weak, the eddies seen in Figure 5 persist, and the net flow has to snake its way between them, as discussed by Jeffrey and Sherwood,[2] Thamida and Chang,[13] and Yossifon *et al.*[14]

VI. CONCLUDING REMARKS

We have shown that the system of induced charge electro-osmotic eddies in a cylindrical pore can have a rich structure that varies markedly with pore aspect ratio. If flows created by induced charge electroosmosis are strong compared to net motion through the pore, there is a danger that fluid trapped in the eddies may become contaminated (or may degrade) over time, and lead to contamination of samples passing through the pore. Such problems can be reduced by suitable choice of pore geometry and imposed electric field strength, in order to control the ratio of eddy velocity to volumetric flow rate through the pore.

ACKNOWLEDGMENTS

We thank Professor E. Yariv (Technion) for helpful suggestions. M.M. and S.G. acknowledge support from the National Institutes of Health (NIH) through Grant No. 4R01HG004842-03. S.G. was hosted by the Cavendish Laboratory, University of Cambridge, as visiting Professor with

funds provided by the Leverhulme Trust. J.D.S. thanks the Department of Applied Mathematics and Theoretical Physics, University of Cambridge, and the Institut de Mécanique des Fluides de Toulouse, for hospitality.

[1] H. K. Moffatt, "Viscous and resistive eddies near a sharp corner," J. Fluid Mech. **18**, 1–18 (1964).
[2] D. J. Jeffrey and J. D. Sherwood, "Streamline patterns and eddies in low-Reynolds number flows," J. Fluid Mech. **96**, 315–334 (1980).
[3] G. I. Taylor, "The formation of emulsions in definable fields of flow," Proc. R. Soc. London, Ser. A **146**, 501–523 (1934).
[4] O. Scrivener, C. Berner, R. Cressely, R. Hocquart, R. Sellin, and N. S. Vlachos, "Dynamical behaviour of drag-reducing polymer solutions," J. Non-Newtonian Fluid Mech. **5**, 475–495 (1979).
[5] M. Cachile, L. Talon, J. M. Gomba, J. P. Hulin, and H. Auradou, "Stokes flow paths separation and recirculation cells in X-junctions of varying angle," Phys. Fluids **24**, 021704 (2012).
[6] M. V. Berry and M. R. Mackley, "The six roll mill: Unfolding an unstable persistently extensional flow," Philos. Trans. R. Soc. A **287**, 1–16 (1977).
[7] M. Mao, S. Ghosal, and G. Hu, "Hydrodynamic flow in the vicinity of a nanopore induced by an applied voltage," Nanotechnology **24**, 245202 (2013).
[8] M. Mao, J. D. Sherwood, and S. Ghosal, "Electroosmotic flow through a nanopore," J. Fluid Mech. **749**, 167–183 (2014).
[9] J. D. Sherwood, M. Mao, and S. Ghosal, "Electroosmosis in a finite cylindrical pore: Simple models of end effects," Langmuir **30**, 9261–9272 (2014).
[10] P. Morse and H. Feshbach, *Methods of Theoretical Physics* (McGraw-Hill, New York, 1953).
[11] O. Schnitzer and E. Yariv, "Strong electro-osmotic flows about dielectric surfaces of zero surface charge," Phys. Rev. E **89**, 043005 (2014).
[12] T. A. Driscoll and L. N. Trefethen, *Schwarz-Christoffel Mapping* (Cambridge University Press, Cambridge, 2002).
[13] S. K. Thamida and H.-C. Chang, "Nonlinear electrokinetic ejection and entrainment due to polarization at nearly insulated wedges," Phys. Fluids **14**, 4315–4328 (2002).
[14] G. Yossifon, I. Frankel, and T. Miloh, "On electro-osmotic flows through microchannel junctions," Phys. Fluids **18**, 117108 (2006).
[15] E. Yariv and M. J. Davis, "Electro-osmotic flows over highly polarizable dielectric surfaces," Phys. Fluids **22**, 052006 (2010).
[16] OpenCFD, *OpenFOAM: The Open Source CFD Toolbox – User's Guide*, 2nd ed. (OpenCFD Ltd., UK, 2012).
[17] U. F. Keyser, B. N. Koeleman, S. van Dorp, D. Krapf, R. M. M. Smeets, S. G. Lemay, N. H. Dekker, and C. Dekker, "Direct force measurements on DNA in a solid-state nanopore," Nat. Phys. **2**, 473–477 (2006).
[18] S. Garaj, W. Hubbard, A. Reina, J. Kong, D. Branton, and J. A. Golovchenko, "Graphene as a subnanometre trans-electrode membrane," Nature (London) **467**, 190–193 (2010).
[19] C. A. Merchant, K. Healy, M. Wanunu, V. Ray, N. Peterman, J. Bartel, M. D. Fischbein, K. Venta, Z. Luo, A. T. C. Johnson, and M. Drndić, "DNA translocation through graphene nanopores," Nano Lett. **10**, 2915–2921 (2010).